Onatoyinbo *et al.*
Sustainable Energy Research (2023) 10:19
https://doi.org/10.1186/s40807-023-00091-y

Sustainable Energy Research

ORIGINAL RESEARCH ARTICLE

Open Access

Comparison of the sensitivities and accuracies of optoelectronic transducers for solar irradiance measurement

Olubunmi O. Onatoyinbo[1,2], Alexander A. Willoughby[1], Ayodele O. Soge[1*] and Oluropo F. Dairo[2]

Abstract

This paper compares the sensitivities and accuracies of four different optoelectronic transducers in measuring solar irradiance for the fabrication of portable and low-cost pyranometers. Trans-impedance conditioning circuits were designed for two phototransistors (BP103 and SFH3310) and two photodiodes (BPW21 and BPW34). The Arduino Mega 2560 was used as an interface between the analogue signal produced by the conditioning circuits and the digital output ports. The transducers with a standard pyranometer RSRA_05V were arranged on a vero board and exposed to the sun. Statistical analysis of the experimental results produced the least root mean square error value of 6.58794 Wm^{-2} for phototransistor BP103 during the dry season followed by 13.35216 Wm^{-2} for phototransistor SFH3310 during the dry season. The correlation coefficients of BPW21, BPW34, BP103, and SFH3310 with the standard pyranometer are 0.9489, 0.9916, 0.9976, and 0.9905, respectively. The experimental results obtained from the phototransistors BP103 and SFH3310 strongly correlated with those of the standard pyranometer coupled with lower root mean square error and mean bias error values than those of the photodiodes. Thus, the phototransistors BP103 and SFH3310 are more accurate and effective for measuring solar irradiance. This study contributes to the development of low-cost and accurate solar radiation meters.

Keywords Phototransistors, Photodiodes, Pyranometer, Solar irradiance, Arduino Mega 2560

Introduction

Solar irradiance is the primary source of energy on the earth and a major contributing factor to several other phenomena such as global or regional climate variations (National Geographic, 2022; Penza et al., 2022), ecosystems (Lean, 2017; Schmutz, 2021), telecommunication (Rocha et al., 2021), and renewable energy applications (Penza et al., 2022). In recent years, diverse solar power systems are continuously installed worldwide as a measure to combat the negative impacts of climate change and global warming caused by greenhouse gases from fossil fuels. The relevance of solar irradiance measurement in optimizing the performance of these power systems cannot be over-emphasized (Al-Rasheedi et al., 2018). For instance, the design of highly efficient solar photovoltaic (PV) systems mostly requires the estimation of global irradiation incidents on the earth's surface. Similarly, solar irradiance measurements are attracting increasing attention in agriculture where impact assessment of solar radiation is of utmost importance (Rocha et al., 2021; Trnka et al., 2007). Moreover, accurate measurements of solar irradiance play a critical role in the development and validation of radiation models widely utilized in solar resource assessments and energy simulations (Al-Rasheedi et al., 2018; Gueymard, 2012; Gueymard & Ruiz-Arias, 2015).

*Correspondence:
Ayodele O. Soge
sogea@run.edu.ng; ayosoge@gmail.com
[1] Department of Physical Sciences, Faculty of Natural Sciences, Redeemer's University, PMB 230, Ede, Osun State, Nigeria
[2] Department of Electrical and Electronic Engineering, Faculty of Engineering, Redeemer's University, PMB 230, Ede, Osun State, Nigeria

Solar radiation can be evaluated either in the form of total solar irradiance outside the earth's atmosphere using satellites or as global solar irradiance at the earth's surface by utilizing ground-based instrumentation such as pyranometers (Roy et al., 2021). Generally, satellite data are usually used in combination with ground data to determine inter-annual variability and long-term mean values (Wilbert et al., 2018). In the construction of a solar power plant, ground measurements normally exhibit incredibly greater accuracies compared to satellite data concerning the general guidelines for choice of location, instrument, system maintenance, and monitoring for optimum performance (Wilbert et al., 2018).

For most system applications, reasonable accuracy at a low cost is usually preferred over high accuracy at a high cost in measuring global solar irradiance. The pyranometers that give accurate readings are quite expensive and hence not used extensively (Patil et al., 2013). Consequently, there is a growing demand for inexpensive devices for accurate monitoring of solar irradiance. In meeting this demand, a wide range of low-cost pyranometers consisting of different optoelectronic devices have been reported by researchers. For instance, Tohsing et al. (2019) developed a low-cost pyranometer by using a phototransistor BPX43-4. Arduino Pro mini ATmega328P microcontroller was used as an analogue–digital converter (ADC). The components were assembled in FB05 for protection against environmental conditions. A Teflon sheet with a thickness of 1.0 mm was used as a solar radiation attenuator to prevent the transducer from saturation. Irradiance obtained from the model pyranometer CM21 and the prototype pyranometer were logged at 2-min intervals. Analysis shows that the sensitivity of the prototype was 1.65 mV/W.m^{-2}, mean bias difference − 14.4%, and root mean square difference 15.5%. The difference might be due to the limitation of the field of view and the non-linearity of spectra between the pyranometers (Tohsing et al., 2019). According to the authors, the sensitivity of the prototype is satisfactory but can be investigated further for greater accuracy. Likewise, Rocha et al., (2021) developed a low-cost, surface solar radiation measurement system utilizing photodiodes BPW34 as transducers with a spectral range of 300–1400 nm integrating Internet of Things technology. The performance of the proposed system strongly correlated with that of the government meteorology station (INMet pyranometer) giving correlation coefficients (R^2) of above 0.95. The authors reported that the solar irradiance meter functions like pyranometers built on thermopiles offering high accuracy, low maintenance cost, and wide applications in climatology and power generation. Moreover, Roy et al., (2021) fabricated a low-cost pyranometer using five phototransistors L14G2 connected in parallel and in series with a load resistor. The phototransistors were evenly placed on a semi-spherical body at an altitude of 11 m. The analogue voltage signal across the load resistor that is proportional to the irradiance level was converted to a digital signal by ATmega32L. The transmitter/receiver circuit was incorporated into the system to transmit the data from a remote area to the base station. The digital output was logged at an interval of 30 min for different weather conditions. Data analysis between the developed system and the standard pyranometer LP PYR 10 shows a mean bias error of − 0.2819 Wm^{-2}, mean square error of 2.40 Wm^{-2}, mean absolute error of 1.27%, and an average directional response error of 6.76%. Their system provides an approach to acquire, compress, and store the solar irradiance signal and transmit it from remote areas to the base station.

Furthermore, Cekon et al. (2016) measured the solar radiant flux based on silicon elements powered by two AA1.5 V batteries. The intensity of sun radiation was monitored by four different types of BPW34 photodiode circuits with high speed and high radiant sensitivity. An output voltage from the conditioning circuits is measured by a 10-bit Analogue-to-Digital converter MCP3008 with the step size set to 300 mV and the resolution of measurement set to 3 Wm^{-2}. A data logger was assembled based on an ATmega328 microcontroller which determines the output voltage of the photodiodes and logs the data to SD card. The Real-Time Clock chip PCF8563 and LED are used to indicate the status of the device. Two standard pyranometers ALMEMO FLA628-S and ALMEMO FLA 613 GS readings were used for the comparison and analysis of the global radiation on the horizontal plane and the global radiation on the vertical plane. The comparison indicated good agreement on the horizontal plane and the comparison for vertical planes approximately matched except in the morning which showed little deviation possibly due to the incidence angle of the sun (Cekon et al., 2016).

Al-Rasheedi et al., (2018) investigated the capability of photodiode sensors in providing low-uncertainty data under harsh environments and over sufficiently long periods to perform a thorough evaluation of the solar resource. Two sensor technologies (thermopile radiometers and photodiodes with rotating shadow bands) for solar irradiance measurement in a desert environment were compared. The analysis of the three components of solar irradiance (global, direct, and diffuse) measured by the two sensor technologies generally showed satisfactory deviations within ± 5% for global and direct components. However, a few larger deviations in direct and global irradiance were recorded at low zenith angles. Additionally, negative bias and intricate patterns were found in the diffuse deviations probably caused by an insufficient

spectral correction of the diffuse reading (Al-Rasheedi et al., 2018). Nevertheless, the deviations obtained from the comparison of the two sensor types are negligibly low to ensure a good assessment of the solar resources under harsh and unstable desert conditions (Al-Rasheedi et al., 2018).

Furthermore, the advent of Arduino has made data acquisition easily possible, and thus, most modern instrumentations are now digital based (Onatoyinbo, 2022). The advantage of digital-based instrumentation cannot be over-emphasized as it gives better output, high accuracy, improved timing, decreased circuit complexity, and easing of data acquisition, manipulation, storage, and interpretation (Onatoyinbo, 2022).

The comparison of solar radiation transducers conducted in this study employs an Arduino module that can accept a series of analogue input signals, then process it based on the microprocessor's command to give the required digital output signals. The design consists of five optoelectronic devices that generate parallel analogue signals to the analogue ports of Arduino. A standard pyranometer RSRA_05V is the fifth device, used to compare and validate the readings from the test optoelectronic devices. The Arduino family is designed for a low voltage of 5 V with a resolution of 0.004882 V/step or volt/bit for the 10-bit analogue input (0 to 1024 steps).

Researchers have reported the measurement of solar irradiance during the two main weather seasons in Nigeria: wet or rainy season and dry or Harmattan season. The wet season is usually from April to October while the dry season is between November and March in southern Nigeria (Willoughby & Osinowo, 2018). In northern Nigeria, the dry season usually lasts for several months, typically from October to May. The wet season normally starts in June and terminates in September. Generally, the solar radiation intensity is lower during the wet season months compared to the dry season months. For instance, Nwankwo and Nnabuchi, (2015) measured global solar radiation in Abakaliki, southeast Nigeria using a locally made pyranometer. Solar irradiance measurements were performed between the hours of 12:00 and 16:00 with intervals of 5 min for dry and rainy seasons. Maximum irradiances of 1095.10 Wm^{-2} and 689.48 Wm^{-2} were recorded for dry and rainy seasons, respectively. Similarly, Medugu and Yakubu, (2011) estimated the monthly solar radiation in Yola, northeast Nigeria, and reported that the maximum values of global solar radiation appear in March, April, and May with 24.38 MJm^{-2} day^{-1}, 24.92 MJm^{-2} day^{-1}, and 24.54 MJm^{-2} day^{-1} respectively, during dry season, while 20.31 MJm^{-2} day^{-1} and 20.77 MJm^{-2} day^{-1} were observed for August and September respectively, during wet season. Likewise, Uko et al. (2016) investigated the effect of weather conditions on solar energy in Rivers State University, south-south Nigeria. It was confirmed that solar energy varies between 47.07 $MJm^{-2}Month^{-1}$ and 113.99 $MJm^{-2}Month^{-1}$ with an annual mean of 87.87. The rainy season months of April to September recorded a low value of 86.69 MJm^{-2} day^{-1}, while the dry season of November to January displayed a high value of 89.05 MJm^{-2} day^{-1}.

Furthermore, Oyelami et al., (2020) reviewed the performance of different pyranometers for solar radiation measurement and reported that the photodiode-based pyranometer is the most suitable device for solar radiation measurement in the developing country due to their low cost, accuracy, and ease of fabrication. This claim is further investigated in this study by evaluating the sensitivities and accuracies of four different optoelectronic transducers in measuring solar irradiance for the fabrication of cost-effective pyranometers. The four devices–two phototransistors (BP103 and SFH3310) and two photodiodes (BPW21 and BPW34)–were chosen based on their attractive features shown in Table 1

The radiant sensitivity area of the photodiodes is 7.5 mm^2 for BPW21 and BPW34 which is much greater than those of the phototransistor BP103 (0.12 mm^2) and for phototransistor SFH3310 (0.29 mm^2) indicating that the photodiodes receive more solar energy than the phototransistors. Also, phototransistor BP103 can withstand an operating temperature range of −40 to + 80 °C which is the smallest but suitable for the weather in southwest Nigeria, the location of this study. The minimum angle of half sensitivity is ± 50° indicating

Table 1 Specifications of the four optoelectronic transducers

Parameters	BP103	SFH3310	BPW21	BPW34
Radiant sensitivity area (mm^2)	0.12	0.29	7.5	7.5
Operating temperature (°C)	−40 to + 80	−40 to + 100	−40 to + 125	−40 to + 100
Range of spectral bandwidth (nm)	420–1130	350–970	420–675	430–1100
Angle of half sensitivity (degree)	± 55	± 75	± 50	± 65
Dark current (nm)	≤ 100	< 50	≤ 30	≤ 30

that the performance of the transducers should be equal to almost 100°.

Although several low-cost optoelectronic transducers for solar irradiance measurement have been reported in the literature, their accuracies are markedly lower than those of expensive standard pyranometers. Therefore, this study aims to develop a low-cost solar radiation meter with a very high accuracy comparable to that of a standard pyranometer. To achieve this, the sensitivities and accuracies of four optoelectronic transducers were compared to those of a standard pyranometer (RSRA-05 V) using statistical analysis tools such as correlation coefficient, the mean bias error, the root mean square error, and the standard deviation to identify suitable optoelectronic transducers for accurate measurements of solar irradiance. The novelty of this study lies in the use of Arduino Mega 2560 with an exceptionally high data logging rate of 6 s which is comparable to those of the standard pyranometers of 1 s (Vamvakas et al., 2020).

Material and methods

The block diagram for the comparison of solar radiation transducers is illustrated in Fig. 1. It consists of six main modules: photodiode or phototransistor, standard pyranometer, conditioning circuit, integrated development environment (IDE), power supply unit/battery, memory, real-time clock (RTC), and output screen (LCD).

The power supply unit/battery delivers 5 V and 10 V to power the solar irradiance measuring system. Transducers transform the solar energy received from the sun into electrical energy which is fed into the conditioning circuits to create the set-point for the output voltage of the transformed solar radiance. The optoelectronic transducers are usually calibrated using a standard pyranometer (RSRA-05 V) with its output connected to one of the analogue inputs of the Arduino Mega 2560 which performs the analogue to digital conversion (ADC). The converted digital signals are fed into the memory (data logger) and to the LCD. The Arduino circuit operates as a processor and does not store data. The digital output data obtained from the Arduino circuit are stored in the

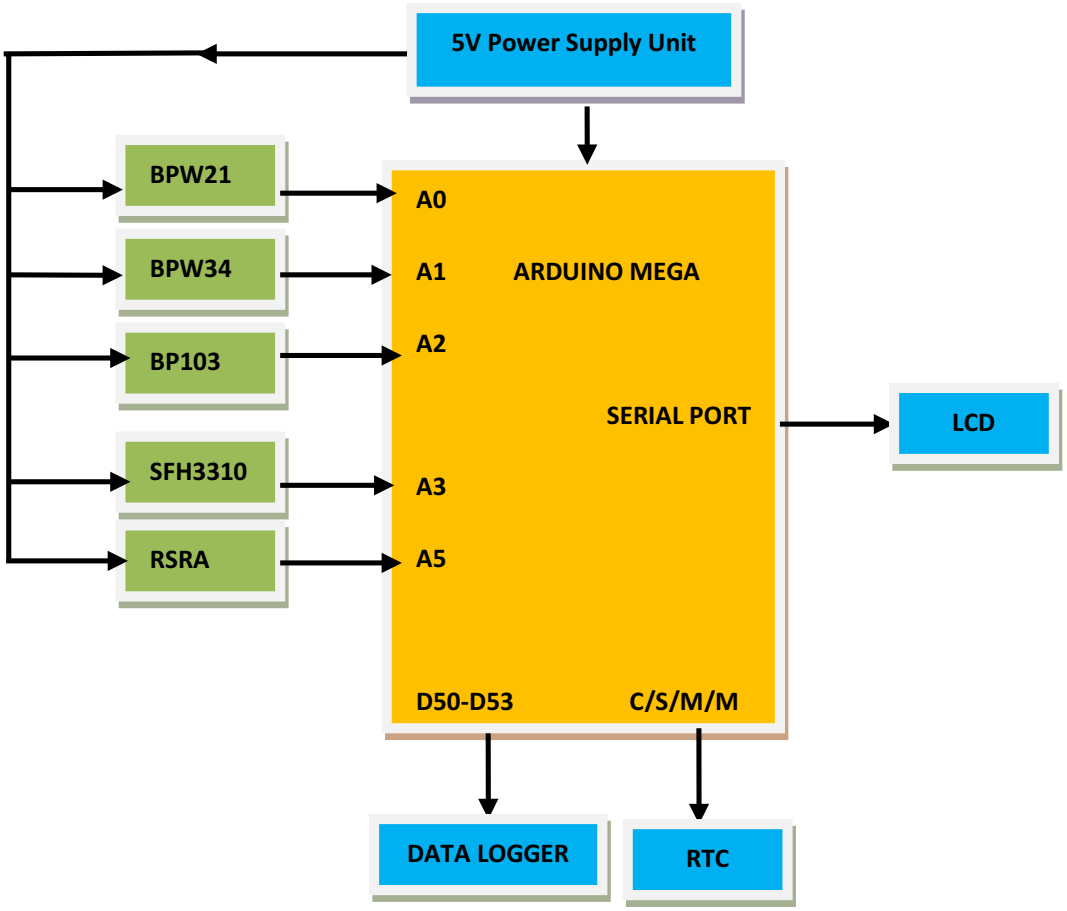

Fig. 1 Block diagram for the comparison of the four solar radiation transducers (BPW21, BPW34, BP103, SFH3310) using a standard pyranometer (RSRA) as the benchmark

memory. The output data from the Arduino circuit are monitored through the output screen.

The comparison of the performance of photo-device transducers is broken into three main steps: (i) design and implementation of conditioning circuits, (ii) implementation of ADC, and (iii) calibration of the set-points.

Design and implementation of conditioning circuits.

The design and the calibration of the conditioning circuit can be classified into three parts: (i) design of photodiodes trans-impedance circuit, (ii) design of phototransistor trans-impedance circuit, and (iii) design of voltage amplification circuit.

Design of photodiode trans-impedance circuit

A photodiode is operated in reversed bias and the leakage current increases in proportion to the amount of light falling on the junction. The output leakage current of a photodiode is fed into the inverting input of an operational amplifier LM358 arranged in trans-impedance form as demonstrated in Fig. 2a. The bandwidth frequency of LM358 is 1 MHz and the breakdown current of the photodiode BPW34 is 100 μA. If R_f is the feedback resistor and I_d

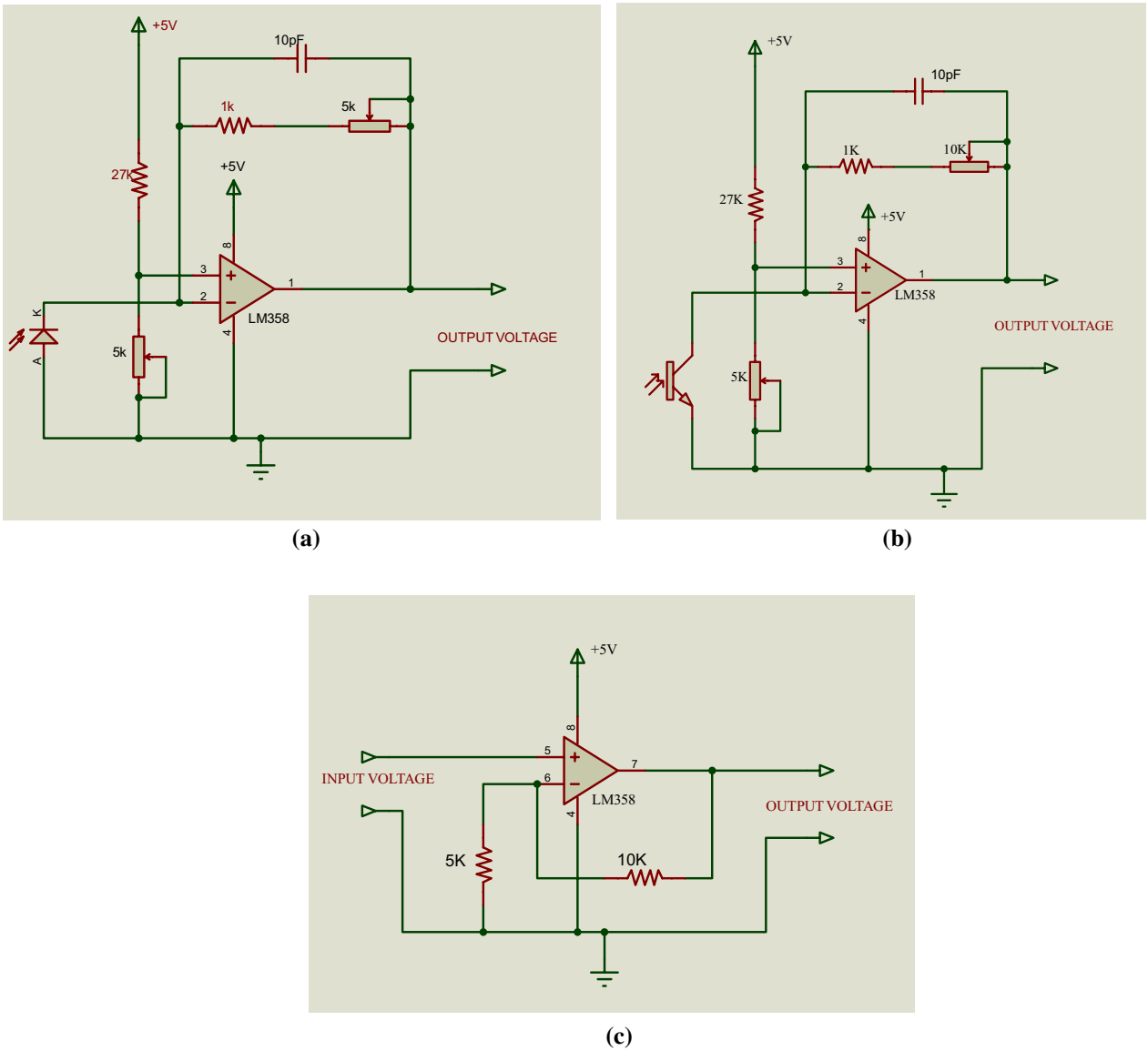

Fig. 2 **a** Photodiode trans-impedance circuit, **b** Phototransistor trans-impedance circuit, and **c** Amplification circuit of the trans-impedance output signal

is the diode current, then Kirchhoff's law is applied to the inverting input of the photodiode trans-impedance circuit in Fig. 2a:

$$I_d R_f \leq 5v. \tag{1}$$

Since $I_d = 100\ \mu A$,

$$R_f \leq 5/\left(10^{-4}\right)\Omega \tag{2}$$

$$R_f \leq 5\left(10^4\right)\Omega.$$

Therefore, 11 kΩ is used for R_f (i.e. 1 kΩ and 10 kΩ connected in series).

To obtain a stable output from the operational amplifier, there is a need to connect a capacitor to the feedback path. For the required capacitor,

$$C \leq \left(2\pi R_f f_b\right)^{-1}, \tag{3}$$

where f_b is the bandwidth frequency is 1 MHz for LM358, and R_f is 11 kΩ. Therefore,

$$C \leq \left[(2\pi)(11)\left(10^3\right)\left(10^6\right)\right]^{-1} F \leq 14.49\ \text{pF}.$$

Thus, a 10 pF capacitor is connected in parallel with the feedback resistor for output stability.

Design of phototransistor trans-impedance circuit

The same trans-impedance circuit was used for both photodiodes (Fig. 2a) and phototransistors (Fig. 2b) since the base junction of a phototransistor is left open and the main difference between photodiode and phototransistor is the current gain. The emitter and the collector of the phototransistor are connected as shown in Fig. 2b.

Design of amplification circuit

The input signal from the transducer is small, which makes the output signal of the trans-impedance circuit small; therefore, signal amplification is necessary. LM358 operational amplifier is used for the amplification as described in Fig. 2c.

A voltage amplification A_v factor of 3 was used since the output voltage of the system cannot be greater than the applied potential. The values of R_1 and R_2 in Fig. 2c were obtained by applying Eq. 4.

$$A_v = 1 + (R_f/R_4), \tag{4}$$

where $R_f = R_2$ and $R_4 = R_1$.

If A_v is 3, and R_4 is selected to be 5 kΩ, then

$$R_f = R_4(A_v - 1)$$

$$R_f = 10k\Omega.$$

The value of the feedback resistor used for the amplification is 10 kΩ.

Figure 3 describes the photograph of the four trans-impedance circuits with the input connectors from the transducers and the output connectors to the analogue input of the Arduino module.

Implementation of the analogue-to-digital converter (ADC)

The precision of the analogue signal obtained from the transducer/trans-impedance circuit was achieved by using an Arduino Mega module shown in Fig. 4. The conditioning output ports as illustrated in Fig. 3 were connected to the analogue inputs $A0$, $A1$, $A2$, and $A3$ of the Arduino Mega 2560.

The pyranometer output is connected to the analogue input $A5$ of the Arduino Mega 2560. Moreover, the Arduino Mega microprocessor was programmed such that it delivers a serial digital output that is stored in the micro-SD card through a micro-SD card adapter.

Calibration of the set-points

For an accurate comparison of the four photoelectric transducers to the standard pyranometer, the set-points of the pot resistors in the conditioning circuits (Fig. 3) must be adjusted. Figure 5 illustrates how the set-point adjustment of the pot resistors was achieved and the photograph of the experimental setup is presented in Fig. 6.

The power supply is used to control the intensity of the lamp, which is fixed at 15 V for a 60-W bulb. The distance between the lamp and the transducer is kept constant at 3 cm. The pyranometer output voltage when the 60-W bulb was fixed at 3 cm to the transducer was found to be 1.03 V. The pyranometer was replaced by the transducer and the set-points of the conditioning circuits were adjusted to obtain the same output voltage of 1.03 V. The adjustments were performed for each of the four transducers.

Techniques for comparing the transducers' data

Mean bias error, root mean square error, and standard deviation are three statistical methods employed in this research to compare the effectiveness of the transducers.

Mean bias error

Mean bias error (MBE) is primarily used to estimate the average bias in the model and to decide if any steps need to be taken to correct the model bias. It also captures the average bias in the prediction. A positive bias error in a variable represents over-estimated data from datasets and vice versa (AgriMetSoft, 2019). Lower values of

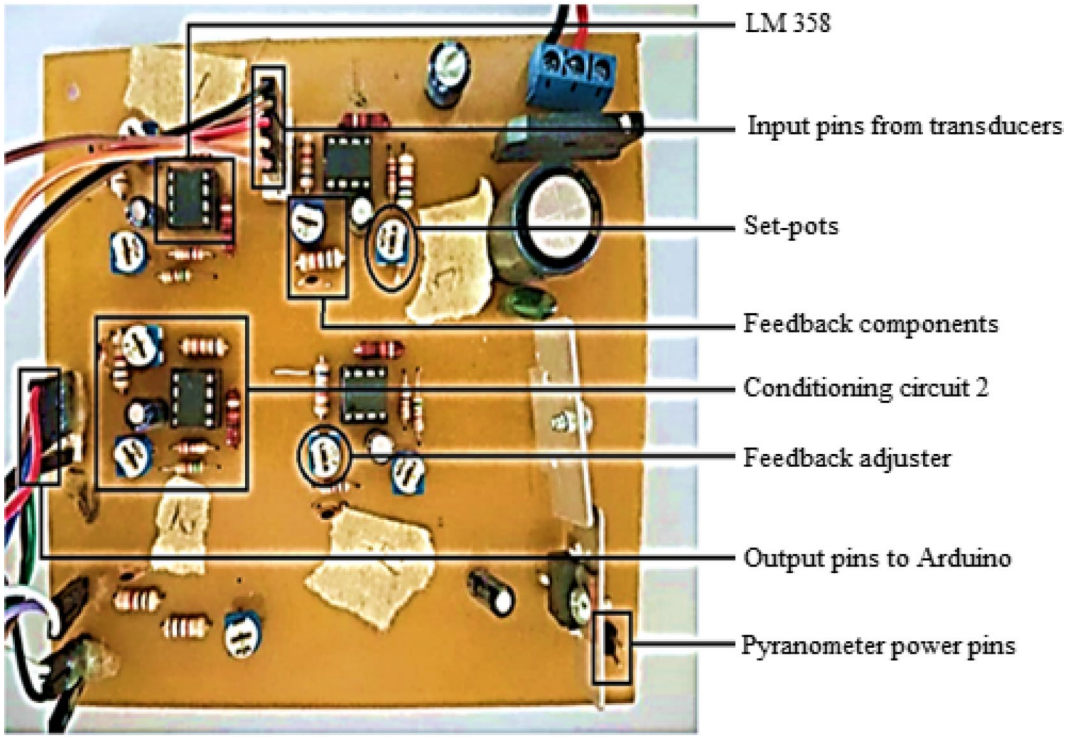

Fig. 3 Four trans-impedance circuits as conditioning circuits

errors and considerably higher values of the correlation coefficient for the variable are of great importance. The statistical relation for mean bias error is given as

$$\mathrm{MBE} = \frac{1}{N}\sum_{i=1}^{N}(E_i - P_i), \tag{5}$$

where N is the total number of data samples, E is the experimental value, and P is the measured value.

Root mean square error

The Root Mean Square Error (RMSE) is a frequently used measure of the difference between values predicted by a model and the values observed from the environment that is being modelled. These individual differences are also called residuals, and the RMSE serves to aggregate them into a single measure of predictive power. RMSE measures the extent of error between two datasets. In other words, RMSE compares a predicted value and an observed or known value (AgriMetSoft, 2019). The statistical relation for RMSE is given as

$$\mathrm{RMSE} = \sqrt{\frac{\sum_{i=1}^{N}(E_i - P_i)^2}{N}}, \tag{6}$$

where N is the total number of data samples, E is the experimental value, and P is the measured value.

Standard deviation

The standard deviation is used to express the statistical variation in the values ascribed to a measured quantity (Wikipedia, 2023). The standard deviation (σ) of solar irradiance measurements obtained from the four opto-electronic transducers and the standard pyranometer was estimated using the statistical relation

$$\sigma = \sqrt{\sum_{i=1}^{N}\frac{(X_i - \mu)^2}{N}}, \tag{7}$$

where X_i is the solar irradiance data, μ is the mean value of the data, and N is the total number of data samples.

Software testing

After the software debugging and the errors were corrected, the software programme was tested on the hardware to determine if communication could be established with the hardware. The arrangement of the setup comprising transducers and the standard pyranometer is displayed in Fig. 7 and was placed where the solar radiation cannot be obstructed. Figure 8 describes how the data logger, SD card module, conditioning circuits, and Arduino board module were connected. The

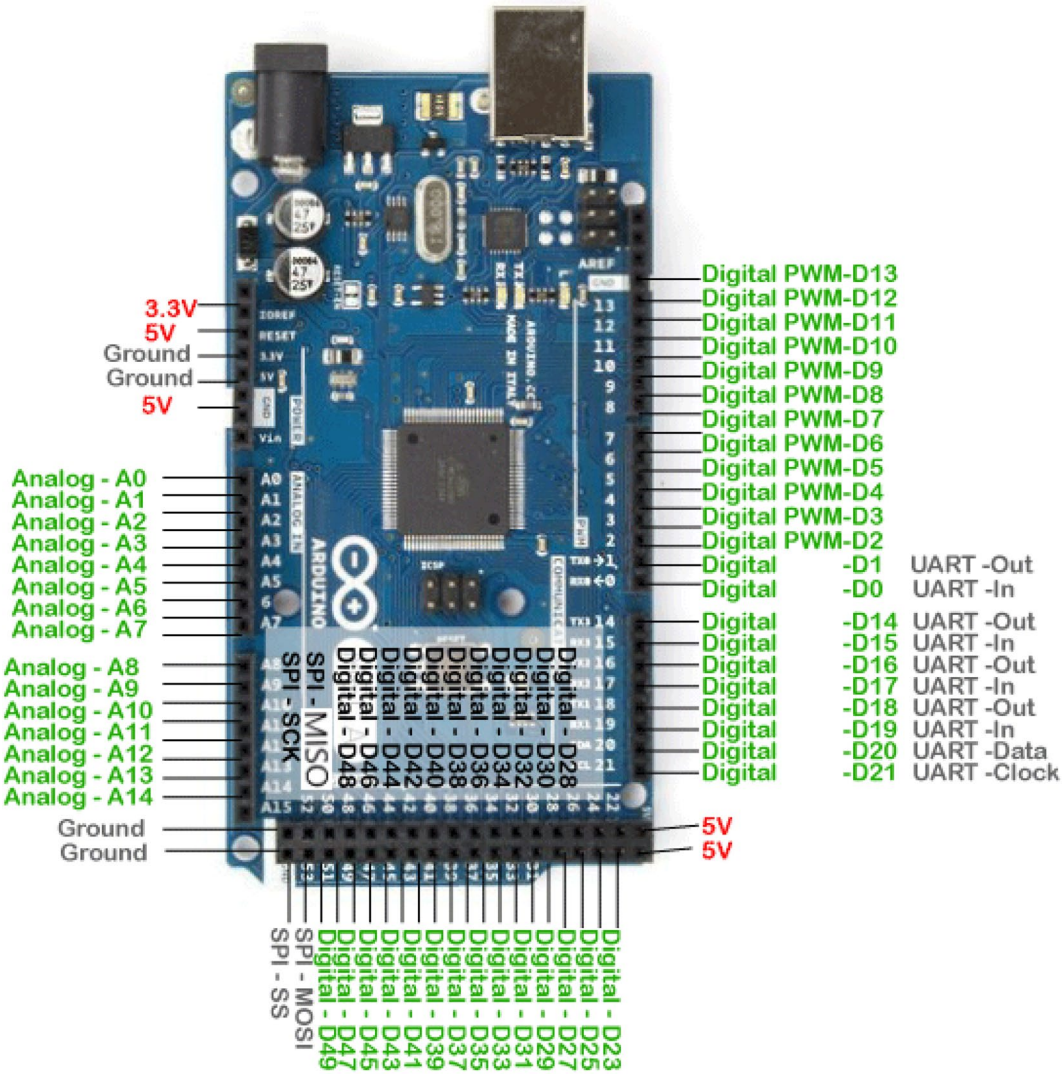

Fig. 4 Arduino Mega 2560 with its input/output pins. (Source: www.instructables.com/Arduino-Serial/)

readings were programmed in such a way to be sampled and logged at 6-s intervals and stored in the SD card.

Results and discussion

Plots of the standard pyranometer (RSRA) output voltage against the output voltage of the transducers were obtained using 500 data points and their linear regression line was determined with their correlation coefficient. Figure 9 shows the RSRA output voltage versus transducer BP103 output voltage. The regression line equation for the plot is given as

$$y = 0.98x_1 + 0.3638. \tag{8}$$

From the experiment in Fig. 5, variable resistors were adjusted such that the output voltage of standard pyranometer RSRA and the trans-impedance circuits were 1.02 V. If the circuit follows the pyranometer's trend, the amplification factor is to be one, the adjustment is to be zero, and the correlation coefficient will be one. The amplification factor is the rate at which the pyranometer's reading responds to the changes in other transducer or trans-impedance readings. Variable x_1 in Eq. 8 is the output voltage of the BP103 trans-impedance circuit, the amplification factor is 0.98, and the adjustment is 0.3638 V. The correlation (R^2) between RSRA and BP103 output voltages is 0.9976.

Similarly, the plot of RSRA output voltage versus transducer BPW21 output voltage is illustrated in Fig. 10.

The regression line equation of the plot is expressed as

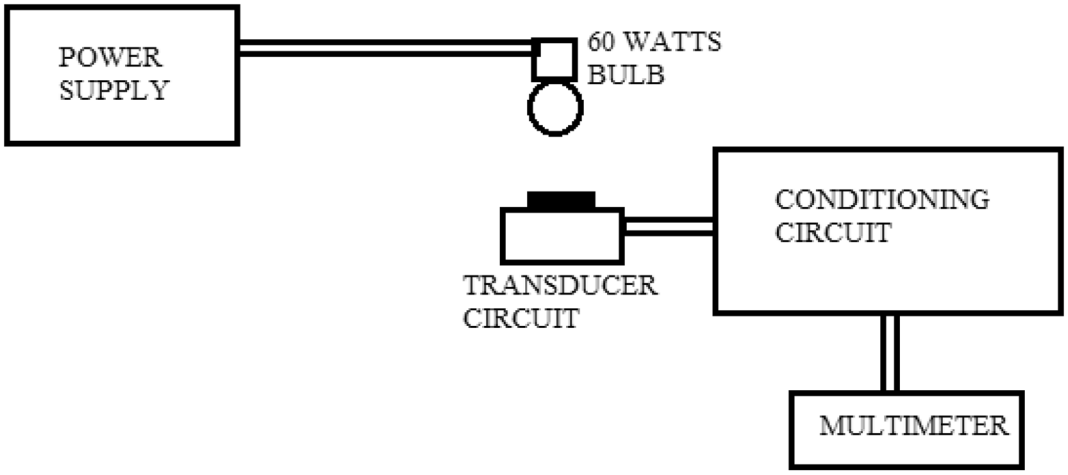

Fig. 5 A schematic diagram for set-point adjustments

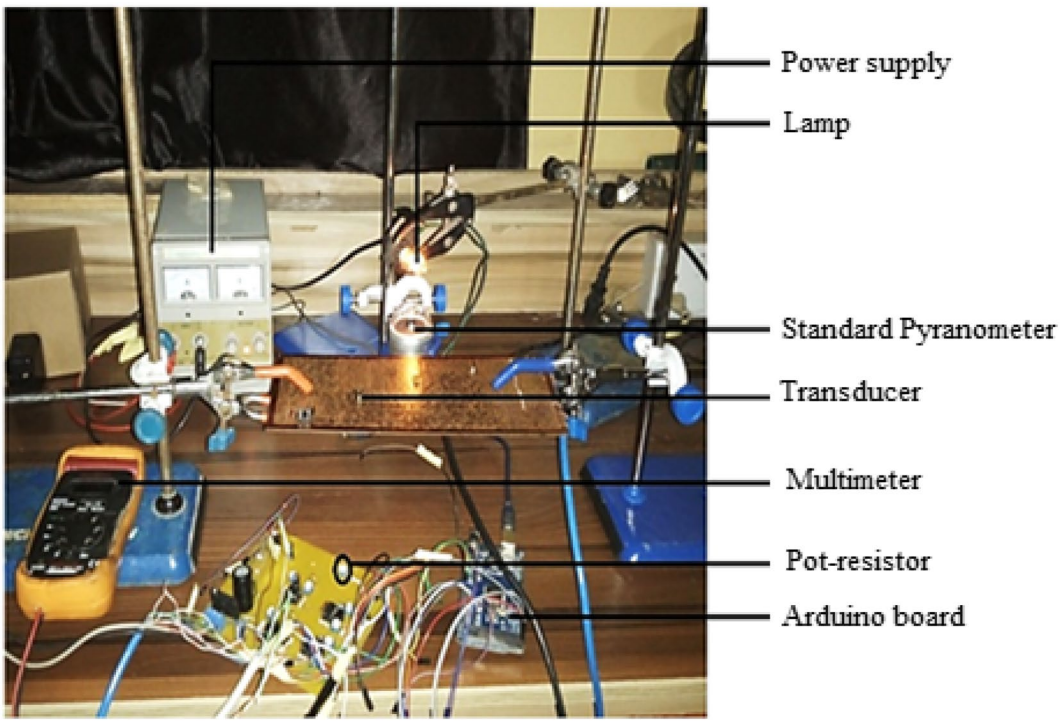

Fig. 6 Experimental setup of the pot resistors set-points

$$y = 13.033x_2 - 9.2824, \tag{9}$$

where x_2 is the output voltage of the BPW21 trans-impedance circuit, the amplification factor is 13.033, and the adjustment is −9.2824 V. The correlation (R^2) between the RSRA output voltage and the BPW21 output voltage is 0.9489.

Additionally, the plot of RSRA output voltage versus transducer BPW34 output voltage is presented in Fig. 11. The regression line equation for the graph is given by

$$y = 65.35x_3 - 52.617, \tag{10}$$

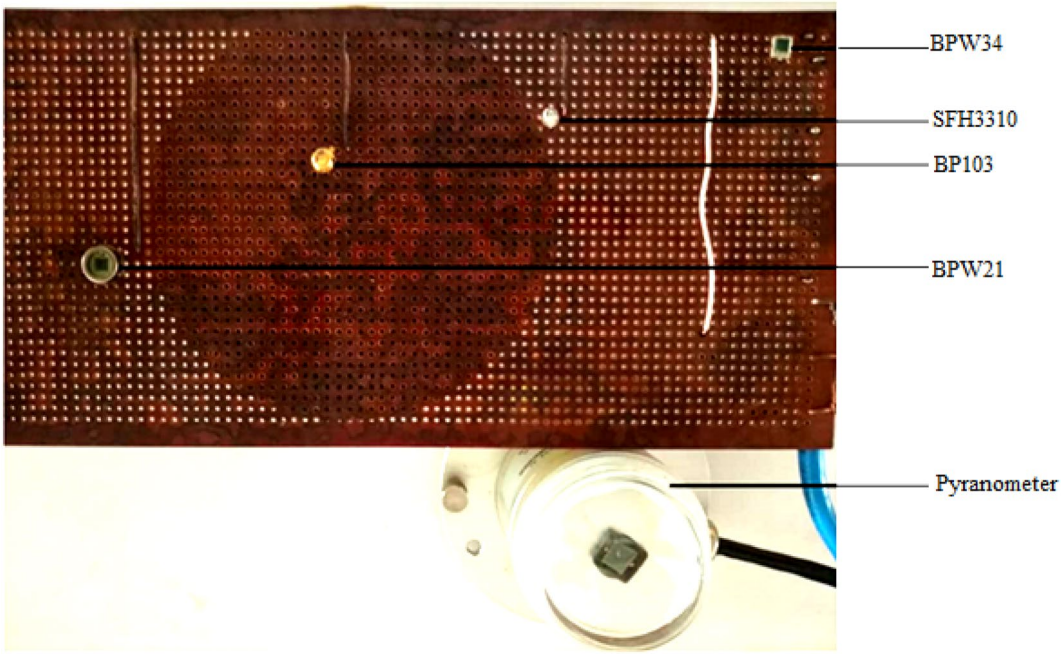

Fig. 7 Assembling of the transducers and the RSRA pyranometer

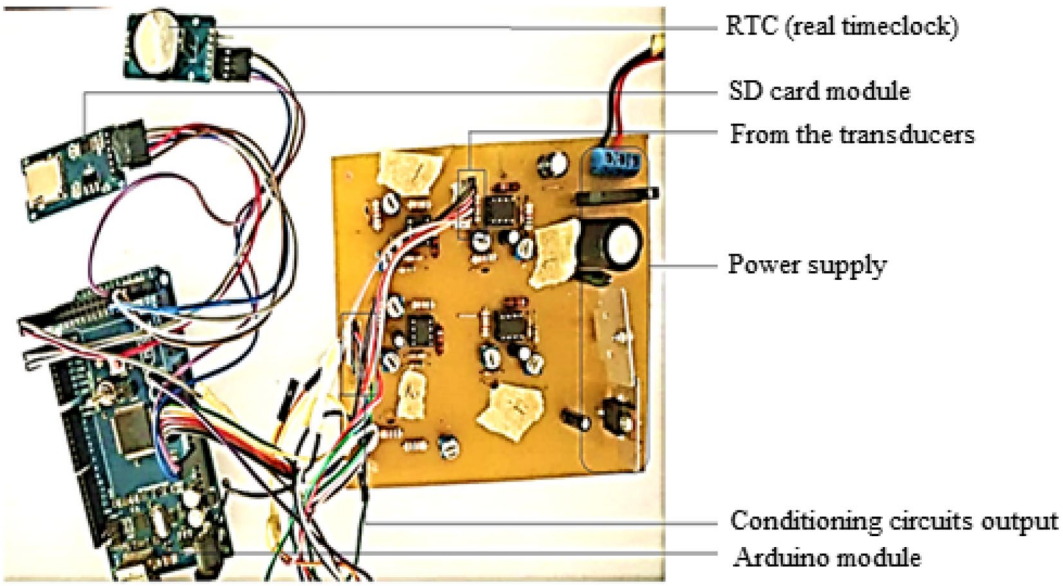

Fig. 8 Connections of the modules

where x_3 is the output voltage of the BPW34 trans-impedance circuit, while the amplification factor is 65.35 and the adjustment is −52.617 V. The correlation (R^2) between RSRA output voltage and BPW34 output voltage is 0.9916. The regression line of RSRA output voltage versus SFH3310 output voltage as depicted in Fig. 12 is

$$y = 1.1009x_4 + 0.0236, \tag{11}$$

where x_4 is the output voltage of the phototransistor SFH3310 trans-impedance circuit. The amplification factor is 1.1009 and the adjustment is 0.0236 V. The correlation between RSRA output voltage and SFH3310 output

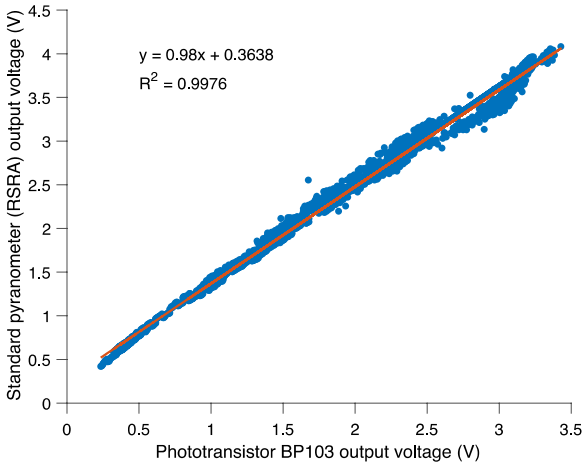

Fig. 9 Plot of Standard Pyranometer versus Phototransistor BP103 output voltages

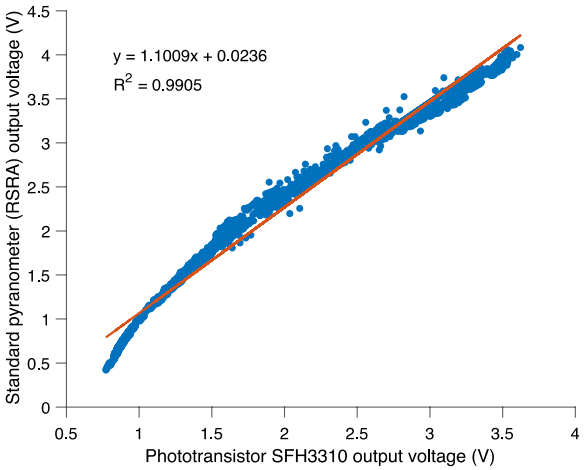

Fig. 12 Plot of Standard Pyranometer versus Phototransistor SFH3310 output voltages

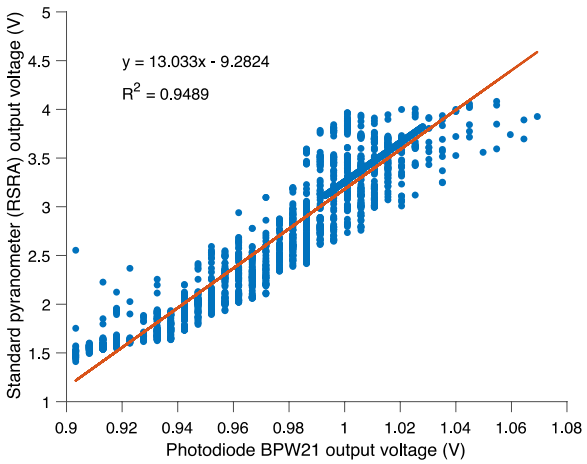

Fig. 10 Plot of Standard Pyranometer RSRA versus Photodiode BPW21 output voltages

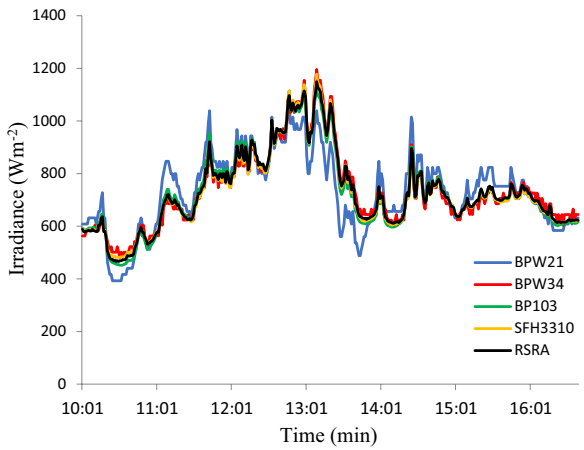

Fig. 13 Plot of Solar irradiance against time for the wet season on 14 October 2021

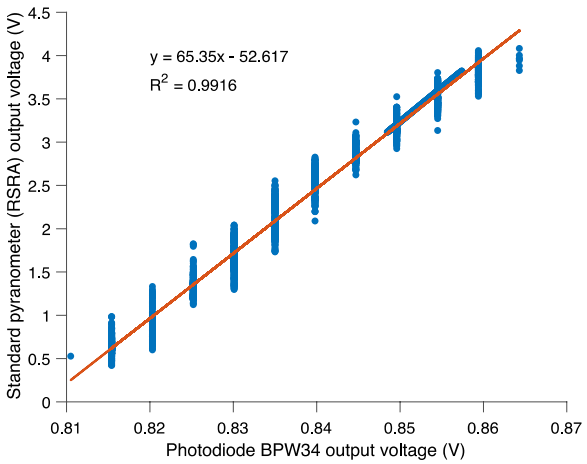

Fig. 11 Plot of Standard Pyranometer versus Photodiode BPW34 output voltages

voltage is 0.9905. Variables x_1, x_2, x_3, and x_4 in Eqs. 8, 9, 10, 11, respectively, are used to calibrate each of the transducer models to that of the standard pyranometer (RSRA). The pyranometer rating of 1 V per 360 Wm^{-2} was used to determine the solar irradiance obtained by the circuits of photodiodes and phototransistors.

According to the regression line parameters obtained from Eqs. 8, 9, 10, 11, the amplification factors of phototransistors BP103 and SFH3310 are almost one. Also, the adjustment values for phototransistors BP103 and SFH3310 are nearly zero. The correlation coefficients (R^2) of BP103 and SFH3310 in comparison to the standard pyranometer RSRA are approximately one compared to the values for photodiodes BPW21 and BPW34.

Furthermore, the solar radiation of the wet season on 14 October 2021 and 20 October 2021 and dry season on

Table 2 Statistical results of the transducers (RMSE and MBE are measured in Wm^{-2})

Date	Statistical methods	Photodiode (BPW21)	Photodiode (BPW34)	Phototransistor (BP103)	Phototransistor (SFH3310)
14 October 2021 (Wet)	RMSE	65.8387	25.4556	14.0569	9.5746
	MBE	5.2338	8.0042	−5.6910	−3.6316
20 October 2021 (Wet)	RMSE	26.3210	17.9658	6.5879	34.4052
	MBE	0.2095	0.119084	−0.1488	8.3233
16 November 2021 (Dry)	RMSE	88.8604	55.9709	22.0249	53.4414
	MBE	−48.7466	−15.2427	3.0164	28.4711
3 January 2022 (Dry)	RMSE	64.0275	40.4330	19.4983	13.3522
	MBE	−22.7869	20.8441	−8.1516	−0.9317

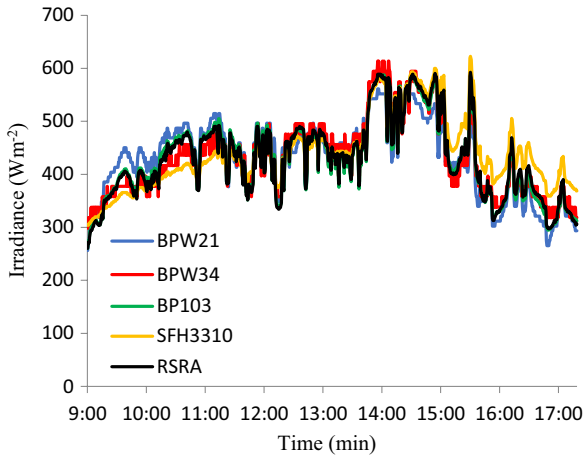

Fig. 14 Plot of Solar irradiance against time for the wet season on 20 October 2021

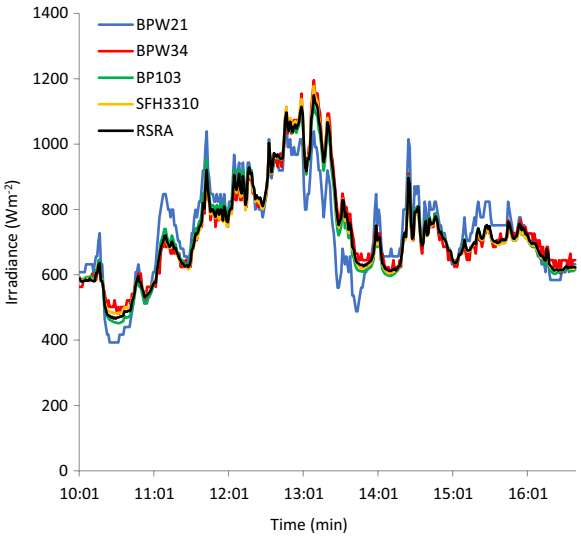

Fig. 16 Plot of Solar irradiance against time for the dry season on 3 January 2022

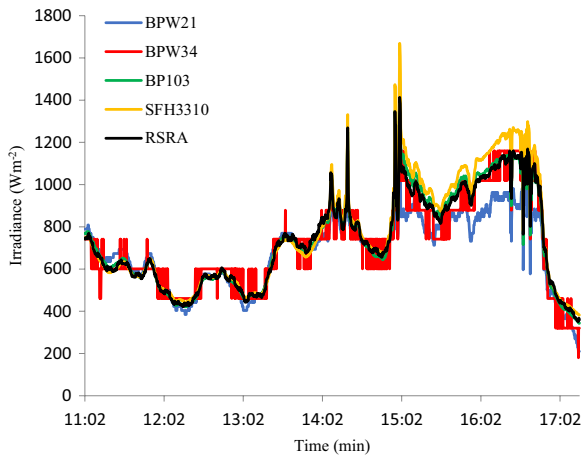

Fig. 15 Plot of Solar irradiance against time for the dry season on 16 November 2021

16 November 2021 and 3 January 2022 at the study location (Ede in southwestern Nigeria, 7° 44′ 20″ N latitude, 4° 26′ 10″ E longitude) was plotted against time and displayed in Figs. 13, 14, 15, 16. The four days chosen for solar irradiance measurement are good representations of the two major weather seasons in Nigeria: the wet season starts in March and ends in October, while the dry season usually begins in November and terminates at the end of February (Nwankwo & Nnabuchi, 2015).

The mean bias error and root mean square error of the four optoelectronic transducers in measuring the solar irradiance of the wet season on 14 October 2021 and 20 October 2021 and dry season on 16 November 2021 and 3 January 2022 at the study location (Redeemer's University, Ede, Southwest Nigeria) are shown in Table 2.

Considering the solar irradiance measurement during the wet season on 14 October 2021, the RMSE value for photodiode BPW21 is 65.8387 Wm^{-2} which is relatively high compared to other optoelectronic transducers.

Table 3 Measurement standard deviations of the transducers and standard pyranometer measured in Wm^{-2}

Date	Standard Pyranometer	Photodiode BPW21	Photodiode BPW34	Phototransistor BP103	Phototransistor SFH3310
14 October 2021 (Wet)	309.4605	230.1520	266.9609	277.2235	303.6276
20 October 2021 (Wet)	74.5291	69.7199	72.3347	74.1812	66.6208
16 November 2021 (Dry)	219.1965	174.2682	218.5445	226.5363	254.6983
3 January 2022 (Dry)	45.5326	62.2752	63.5853	46.8241	61.4530

Similarly, the RMSE for phototransistor SFH3310 is 9.5747 Wm^{-2} indicating that the phototransistor correlates strongly with the standard pyranometer RSRA.

On the wet day of 20 October 2021, the degree of correlation is significant between 11:21 and 14:27 with solar irradiance of 386.712 Wm^{-2} and 537.876 Wm^{-2}, respectively, except for photodiode BPW34 that deviates (Fig. 14). There is a significant difference between the solar irradiance measurements of the four optoelectronic transducers and that of the standard pyranometer RSRA at 09:00–11:21 and 15:05–17:00 (Fig. 14). Despite the difference, photodiode BPW34 has the minimum MBE value of 0.1191 Wm^{-2}. However, phototransistor BP103 has an RMSE value of 6.5879 Wm^{-2} indicating a good correlation with the standard pyranometer compared to other transducers with higher RMSE values.

Moreover, there is a strong correlation between phototransistor BP103 and standard pyranometer RSRA on the dry day of 16 November 2021 (Fig. 15) with MBE of 3.0164 Wm^{-2} and RMSE of 22.0249 Wm^{-2} (Table 2) which implies that BP103 has a very good sensitivity at that period and is suitable for pyranometer transducer. As illustrated in Fig. 15, the four transducers have strong correlations with the standard pyranometer RSRA from 09:02 to 14:54, but there is a marked difference in irradiance measurements between 14:54 and 17:02. Photodiodes BPW21 and BPW34 exhibit MBE of -48.7466 Wm^{-2} and -15.2427 Wm^{-2}, respectively, suggesting that the transducers over-estimated the measured data which may be largely due to dusty atmosphere or any other weather condition. Phototransistor SFH3310 with MBE of 28.4711 Wm^{-2} demonstrates that the transducer under-estimated the measured data which could be attributed to solar radiation angle of incidence or weather conditions.

Furthermore, phototransistors BP103 and SFH3310 exhibited a strong correlation with the standard pyranometer RSRA in measuring the solar irradiance on the dry day of 3 January 2022 as depicted in Fig. 16. The RMSE value for BP103 and SFH3310 were 19.4983 Wm^{-2} and 13.3521 Wm^{-2}, respectively, while the photodiodes displayed higher RMSE values 64.0275 Wm^{-2} and 40.4330 Wm^{-2} for BPW21 and BPW34, respectively. Between the hours of 12:21 and 13:28, there was a significant difference in irradiance measurements by the standard pyranometer and the transducers except for phototransistor BP103 which may be due to variation in temperature.

Table 4 The cost of fabricating a phototransistor-based pyranometer

Items	Price (US dollar)
Phototransistor BP103	0.43
Dual operational amplifier LM358	0.43
5 KΩ ¼ W Pot-resistor	0.66
27 KΩ ¼ W resistor	0.11
1 KΩ ¼ W resistor	0.11
10 pF non-polarized capacitor	0.11
Copper board (4 cm × 4 cm)	0.43
Packaging	2.17
Total cost	**4.45**

The measurement standard deviations of the four optoelectronic transducers are compared to those of the standard pyranometer RSRA as depicted in Table 3.

The measurement standard deviations of the four transducers on wet days of 14 October 2021 and 20 October 2021 are relatively lower than that of the standard pyranometer (Table 3). The lowest standard deviation of 66.62 Wm^{-2} in the solar irradiance measurements was delivered by phototransistor SFH3310 on the wet day of 20 October 2021. Similarly, photodiodes BPW21 and BPW34 displayed standard deviations of 174.29 and 218.54 Wm^{-2}, respectively, lesser than that of the standard pyranometer, for the solar irradiance measurements captured on the dry day of 16 November 2021. However, the standard pyranometer exhibited the lowest standard deviation of 45.53 Wm^{-2} in the measurement of solar irradiance on the dry day of 3 January 2022, closely followed by phototransistor BP103 with a standard deviation of 46.82 Wm^{-2}.

Moreover, to demonstrate the cost-effectiveness of the proposed pyranometer compared to a standard pyranometer, the price of fabricating the proposed pyranometer using phototransistor BP103 is presented in Table 4. While the cost of a standard pyranometer is 95 US dollars (excluding shipping fees and import duties), a locally fabricated phototransistor-based pyranometer costs just a modest sum of 4.45 US dollars. Hence, the proposed pyranometer is much cheaper than the standard pyranometer RSRA_05 V.

Conclusion

The sensitivities and accuracies of four optoelectronic transducers–two phototransistors (BP103 and SFH3310) and two photodiodes (BPW21 and BPW34)–have been compared to those of a standard pyranometer RSRA. Arduino Mega 2560 was used as an interface between the analogue signal produced by the conditioning circuits and the digital output ports. In this study, the use of Arduino Mega 2560 with an exceptionally high data logging rate of 6 s which is comparable to those of the standard pyranometers of 1 s was demonstrated. Statistical analysis was carried out using the correlation coefficient (R^2), the mean bias error (MBE), and the root mean square error (RMSE) to compare the performance of the optoelectronic transducers to that of the standard pyranometer. The significant findings of this study are the following:

- The correlation coefficients of BPW21, BPW34, BP103, and SFH3310 in comparison to standard pyranometer RSRA are 0.9489, 0.9916, 0.9976, and 0.9905, respectively.
- Phototransistor SFH3310 displayed the lowest RMSE values of 9.5747 and 13.3521 Wm^{-2} on the wet day of 14 October 2021 and dry day of 3 January 2022, respectively, indicating that the phototransistor correlates strongly with the standard pyranometer RSRA.
- Similarly, phototransistor BP103 recorded the lowest RMSE values of 6.5879 Wm^{-2} on the wet day of 20 October 2021, signifying a good correlation with the standard pyranometer compared to other transducers with higher RMSE values.
- A strong correlation was observed between phototransistor BP103 and standard pyranometer RSRA on the dry day of 16 November 2021 with the lowest MBE of 3.0164 Wm^{-2} and the lowest RMSE of 22.0249 Wm^{-2}, implying that the phototransistor has an outstanding sensitivity at that period which qualifies it for pyranometer transducer.
- Therefore, based on the experimental results obtained, phototransistors BP103 and SFH3310 are more accurate and effective in measuring solar irradiance than the photodiodes BPW21 and BPW34.

Abbreviations

LCD	Liquid crystal display
LED	Light emitting diode
PV	Photovoltaic
ADC	Analogue-to-digital converter
INMet	International Metrology
MBE	Mean bias error
RMSE	Root mean square error
IDE	Integrated development environment
RTC	Real-time clock
$MJm^{-2}Day^{-1}$	Mega Joule per square metre per day
Eq.	Equation
Wm^{-2}	Watts per square metre
I_d	Diode current
R_f	Feedback resistor
f_b	Bandwidth frequency
C	Capacitance
A_v	Voltage amplification
N	Total number of data samples
E	Experimental value
P	Measured value
σ	Standard deviation:
X_i	Solar irradiance data
μ	Mean value of solar irradiance data

Subscripts

d	Diode
f	Feedback
b	Bandwidth
v	Voltage
i	Non-zero positive integers

Acknowledgements

Not applicable.

Author contributions

AAW conceptualized, designed, and supervised the project. OOO performed the experiments. OOO, AOS, and OFD analysed the data and wrote the manuscript. All the authors edited and approved the manuscript.

Funding

Not applicable.

Availability of data and materials

Not applicable.

Declarations

Competing interests

No potential conflict of interest was reported by the author(s).

Received: 8 August 2023 Accepted: 17 November 2023
Published online: 05 December 2023

References

AgriMetSoft. (2019). *Online Calculators*. Retrieved May 14, 2021, from https://agrimetsoft.com/calculators

Al-Rasheedi, M., Gueymard, C., Ismail, A., & Hussain, T. (2018). Comparison of two sensor technologies for solar irradiance measurement in a desert environment. *Solar Energy, 161*, 194–206.

Cekon, M., Slavik, R., & Juras, P. (2016). Obtainable method of measuring the solar radiant flux based on silicone photodiode element. *Applied Mechanics and Materials, 824*, 477–484.
Gueymard, C. (2012). Clear-sky irradiance predictions for solar resource mapping and large-scale applications: Improved validation methodology and detailed performance analysis of 18 broadband radiative models. *Solar Energy, 86*(8), 2145–2169.
Gueymard, C., & Ruiz-Arias, J. (2015). Validation of direct normal irradiance predictions under arid conditions: A review of radiative models and their turbidity-dependent performance. *Renew. Sust. Energy Rev., 45*, 379–396.
Lean, J. (2017). *Sun-Climate Connections, Oxford Research Encyclopedia of Climate Science*. Oxford Universiy Press.
Medugu, D., & Yakubu, D. (2011). Estimation of mean monthly global solar radiation in Yola – Nigeria using Angstrom model. *Advances in Applied Science Research, 2*(2), 414–421.
National Geographic, N. (2022). *The Power of the Sun*. Retrieved 5 December 2022, from https://education.nationalgeographic.org/resource/power-sun
Nwankwo, S., & Nnabuchi, M. (2015). Global solar radiation measurement in Abakaliki Ebonyi state Nigeria using locally made pyranometer. *International Journal of Energy and Environmental Research, 3*(2), 47–54.
Onatoyinbo, O. (2022). *Comparison of the sensitivities of four photoelectric transducers for irradiance meter. MPhil thesis, Department of Physical Sciences, Faculty of Natural Sciences, Redeemer's University,*. Ede, Nigeria.
Oyelami, S., Azeez, N. A., Adedigba, S. A., Akinola, O. J., & Ajayi, R. M. (2020). A pyranometer for solar radiation measurement-review. *Adeleke University Journal of Engineering and Technology, 3*(1), 61–68.
Patil, A., Haria, K., & Pashte, P. (2013). Photodiode based pyranometer. *International Journal of Advances in Science Engineering and Technology, 1*(1), 29–33.
Penza, V., Berrilli, F., Bertello, L., Cantoresi, M., Criscuoli, S., & Giobbi, P. (2022). Total Solar Irradiance during the Last Five Centuries. *The Astrophysical Journal, 937*(84), 12.
Rocha, A., Fernandes, E., Santos, C., Diniz, J., & Junior, W. (2021). Development of a real-time surface solar radiation measurement system based on the Internet of Things (IoT). *Sensors, 21*(11), 3836.
Roy, S., Panja, S., & Patra, S. (2021). An embedded system to measure ground-based solar irradiance signal. *Measurement, 173*, 108598.
Schmutz, W. K. (2021). Changes in the Total Solar Irradiance and climatic effects. *Journal of Space Weather and Space Climate, 11*, 40.
Tohsing, K., Phaisathit, D., Pattarapanitchai, S., Masiri, I., Buntoung, S., Aumporn, O., & Wattan, R. (2019). A development of a low-cost pyranometer for measuring broadband solar radiation. *Journal of Physics: Conference Series, 1380*(1), 012045.
Trnka, M., Eitzinger, J., Kapler, P., Dubrovský, M., Semerádová, D., Žalud, Z., & Formayer, H. (2007). Effect of estimated daily global solar radiation data on the results of crop growth models. *Sensors, 7*(10), 2330–2362.
Uko, E. D., Otugo, V. N., Sigalo, F. B., & Udonam-Inyang, U. E. (2016). Investigation of the effect of weather conditions on solar energy in rivers state University of Science and Technology, Port Harcourt, Nigeria. *Journal of Atmosphere, Conscientia Beam, 2*(1), 9–16.
Vamvakas, I., Salamalikis, V., & Kazantzidis, A. (2020). Evaluation of enhancement events of global horizontal irradiance due to clouds at Patras, South-West Greece. *Renewable Energy, 151*, 764–771.
Wikipedia. (2023). *Standard Deviation*. Retrieved September 27, 2023, from https://en.wikipedia.org/wiki/Standard_deviation
Wilbert, S., Geuder, N., Schwandt, M., Kraas, B., Jessen, W., Meyer, R., & Nouri, B. (2018). *Best Practices for Solar Irradiance Measurements with Rotating Shadowband Irradiometers: A report of IEA SHC Task 46, Solar Resource Assessment.*
Willoughby, A. A., & Osinowo, M. O. (2018). Development of an electronic load IV curve tracer to investigate the impact of Harmattan aerosol loading on PV module performance in southwest Nigeria. *Solar Energy, 166*, 171–180.

Publisher's Note